Circulation

ORIGINAL RESEARCH ARTICLE

Fibroblast-Specific Proteotranscriptomes Reveal Distinct Fibrotic Signatures of Human Sinoatrial Node in Nonfailing and Failing Hearts

Anuradha Kalyanasundaram, PhD; Ning Li, MD, PhD; Miranda L. Gardner, PhD; Esthela J. Artiga, MS; Brian J. Hansen, PhD; Amy Webb, PhD; Michael A. Freitas, PhD; Maciej Pietrzak, PhD; Bryan A. Whitson, MD, PhD; Nahush A. Mokadam, MD; Paul M.L. Janssen, PhD; Peter J. Mohler, PhD; Vadim V. Fedorov, PhD

BACKGROUND: Up to 50% of the adult human sinoatrial node (SAN) is composed of dense connective tissue. Cardiac diseases including heart failure (HF) may increase fibrosis within the SAN pacemaker complex, leading to impaired automaticity and conduction of electric activity to the atria. Unlike the role of cardiac fibroblasts in pathologic fibrotic remodeling and tissue repair, nothing is known about fibroblasts that maintain the inherently fibrotic SAN environment.

METHODS: Intact SAN pacemaker complex was dissected from cardioplegically arrested explanted nonfailing hearts (non-HF; n=22; 48.7±3.1 years of age) and human failing hearts (n=16; 54.9±2.6 years of age). Connective tissue content was quantified from Masson trichrome–stained head-center and center-tail SAN sections. Expression of extracellular matrix proteins, including collagens 1 and 3A1, CILP1 (cartilage intermediate layer protein 1), and POSTN (periostin), and fibroblast and myofibroblast numbers were quantified by in situ and in vitro immunolabeling. Fibroblasts from the central intramural SAN pacemaker compartment (≈10×5×2 mm^3) and right atria were isolated, cultured, passaged once, and treated ± transforming growth factor β1 and subjected to comprehensive high-throughput next-generation sequencing of whole transcriptome, microRNA, and proteomic analyses.

RESULTS: Intranodal fibrotic content was significantly higher in SAN pacemaker complex from HF versus non-HF hearts (57.7±2.6% versus 44.0±1.2%; $P<0.0001$). Proliferating phosphorylated histone 3^+/vimentin$^+$/CD31$^-$ (cluster of differentiation 31) fibroblasts were higher in HF SAN. Vimentin$^+$/α-smooth muscle actin$^+$/CD31$^-$ myofibroblasts along with increased interstitial POSTN expression were found only in HF SAN. RNA sequencing and proteomic analyses identified unique differences in mRNA, long noncoding RNA, microRNA, and proteomic profiles between non-HF and HF SAN and right atria fibroblasts and transforming growth factor β1–induced myofibroblasts. Specifically, proteins and signaling pathways associated with extracellular matrix flexibility, stiffness, focal adhesion, and metabolism were altered in HF SAN fibroblasts compared with non-HF SAN.

CONCLUSIONS: This study revealed increased SAN-specific fibrosis with presence of myofibroblasts, CILP1, and POSTN-positive interstitial fibrosis only in HF versus non-HF human hearts. Comprehensive proteotranscriptomic profiles of SAN fibroblasts identified upregulation of genes and proteins promoting stiffer SAN extracellular matrix in HF hearts. Fibroblast-specific profiles generated by our proteotranscriptomic analyses of the human SAN provide a comprehensive framework for future studies to investigate the role of SAN-specific fibrosis in cardiac rhythm regulation and arrhythmias.

Key Words: extracellular matrix ■ fibroblasts ■ fibrosis ■ heart failure ■ proteomics ■ sinoatrial node ■ transcriptome

Correspondence to: Vadim V. Fedorov, PhD, Department of Physiology and Cell Biology, The Ohio State University Wexner Medical Center, 5196 Graves Hall, 333 W 10th Ave, Columbus, OH 43210-1218. Email vadim.fedorov@osumc.edu

The Data Supplement is available with this article at https://www.ahajournals.org/doi/suppl/10.1161/CIRCULATIONAHA.120.051583.

For Sources of Funding and Disclosures, see page 142.

Circulation is available at www.ahajournals.org/journal/circ

Clinical Perspective

What Is New?

- The study provides a quantitative atlas of unique transcriptomic and proteomic signatures of nonfailing and failing human sinoatrial node (SAN) fibroblasts.
- In the failing human SAN, myofibroblasts, CILP1 (cartilage intermediate layer protein 1), and POSTN (periostin) are found within increased interstitial fibrosis.
- Our data provide a comprehensive fibroblast-specific molecular framework to determine the mechanisms and role of SAN-specific extracellular matrix composition in SAN function and dysfunction.

What Are the Clinical Implications?

- These comprehensive human fibroblast–specific data sets can be used to define the contribution of intranodal fibrotic content to SAN normal pacemaker function and for designing biological pacemakers.
- Isolated fibroblasts identify a novel cellular platform to study SAN and atrial fibrosis and arrhythmias in human heart failure.
- Proteotranscriptomic data sets can be used to identify novel human SAN fibroblast-specific molecular and protein targets to develop antifibrotic strategies targeting SAN dysfunctions and atrial arrhythmias.

Nonstandard Abbreviations and Acronyms

Akt	protein kinase B
αSMA	α-smooth muscle actin
CADH2	cadherin2
CD31	cluster of differentiation 31
CILP1	cartilage intermediate layer protein 1
COL3A1	collagen 3A1
ECM	extracellular matrix
HF	heart failure
ITA4	integrin-α4
ITPR2	inositol 1,4,5-trisphosphate receptor
JAK	Janus kinase
KEGG	Kyoto Encyclopedia of Genes and Genomes
lncRNA	long noncoding RNA
LTBP2	latent transforming growth factor binding protein
miRNA	microRNA
PHH3	phosphorylated histone H3
PI3K	phosphoinositide 3-kinase
POSTN	periostin
RA	right atrium
RET1	retinol binding protein
SAN	sinoatrial node
STAT1	signal transducer and activator of transcription 1
STAT2	signal transducer and activator of transcription 2
SYNE1	nesprin
TGFβ1	transforming growth factor β1
TLN1	talin1

The sinoatrial node (SAN), the primary pacemaker of the human heart, is a heterogeneous composition of specialized pacemaker cardiomyocytes and nonexcitable cells (eg, fibroblasts).[1,2] Histologic postmortem evaluations[3] and recent structural in vivo and ex vivo 3D electrostructural imaging of human hearts have demonstrated that the distinctive 3D intramural structure of the human SAN pacemaker complex is primarily composed of dense connective tissue.[1,4,5] Even healthy human SANs are composed of 35% to 55% dense connective tissue, from ≈24% in infants with age-induced increases up to ≈60% in elderly hearts,[6] which is unique for humans versus animals.[4,7] Such high levels of extracellular matrix (ECM) would be considered pathologic in any other cardiac region, which could lead to arrhythmias and conduction impairments. In contrast, the distinctive high level of ECM in the SAN is required to electrically insulate pacemaker cardiomyocytes to maintain source–sink balance leading to activation of the large right atrial (RA) myocardium by the relatively small SAN pacemaker complex.[4] The cellular basis and molecular mechanisms driving the naturally high fibrotic levels in human SAN is a terra incognita. No study has examined SAN fibroblasts, the primary cellular source of connective tissue, to determine whether there are quantitative and qualitative characteristics that uniquely enable them to secrete and maintain the high levels of connective tissue found in the SAN.

SAN ECM is known to increase in several human diseases, including heart failure (HF), which is associated with cardiac arrhythmias and impairment of SAN automaticity, eventually leading to SAN dysfunction.[3,4,8,9] Recent ex vivo near-infrared optical mapping studies of diseased human hearts show that SAN fibrosis could specifically interrupt automaticity and introduce conduction blocks by disrupting electric connectivity between SAN pacemaker clusters and conduction pathways[5,10,11] (Figure 1A). Whereas clinical and experimental studies have clearly emphasized the critical role of SAN fibrosis as a causal factor of SAN dysfunction, the cellular and molecular basis for the intriguing levels of dense connective tissue in the healthy SAN and pathophysiologic HF-induced SAN fibrosis upregulation has never been studied.

Almost all of our understanding regarding cardiac fibrosis, fibroblasts, and their differentiated states, including myofibroblasts, comes from studies of acute

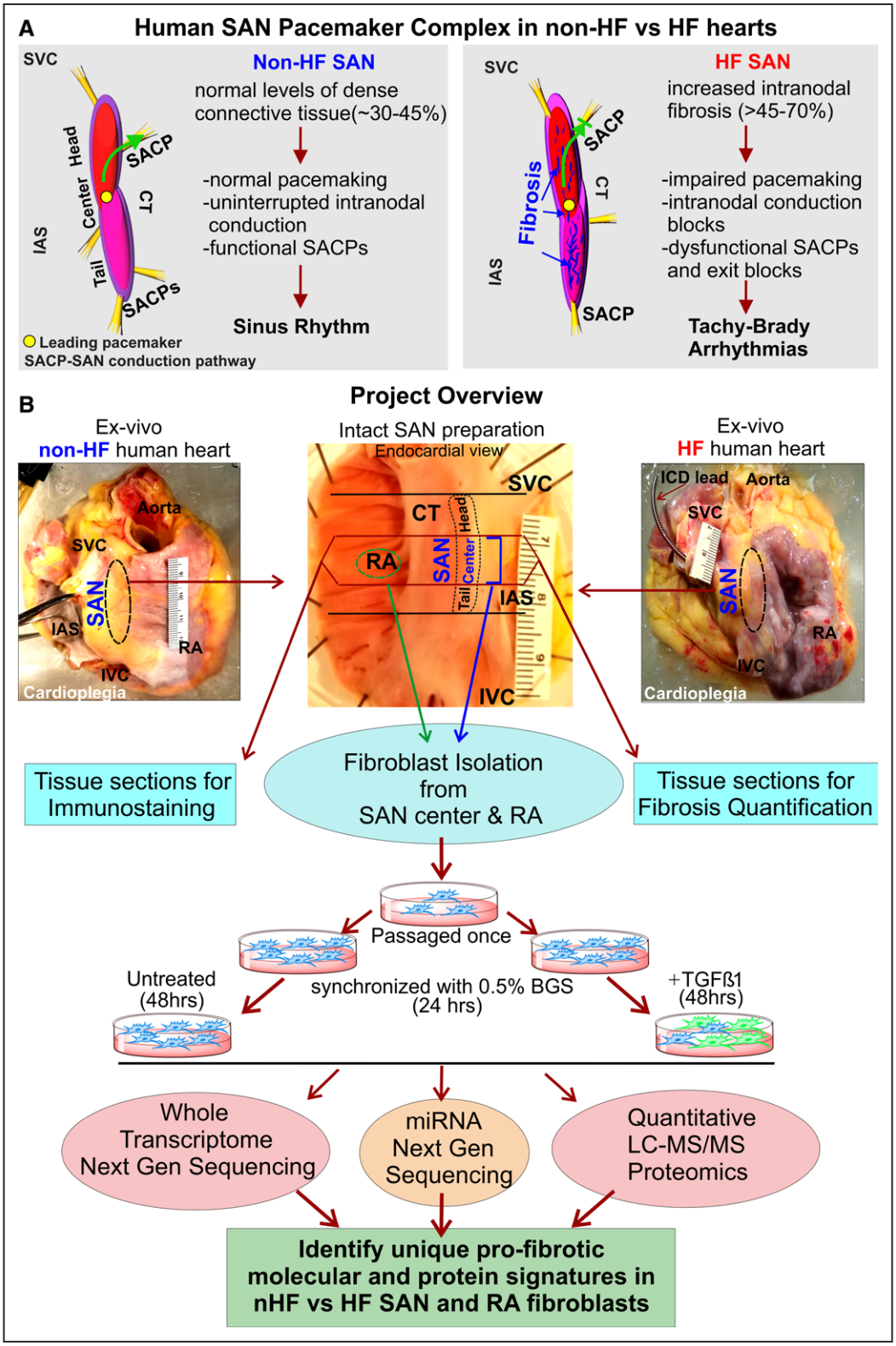

Figure 1. Project description and overview of workflow.
A, Three-dimensional models of nonfailing human sinoatrial node (SAN) pacemaker complex (**left**) and heart failure (HF; **right**) depicting their functional/dysfunctional and structural characteristics. The green arrow shows preferential conduction from the leading pacemaker in the SAN to atria through the SAN conduction pathway (SACP) in non-HF hearts; the blocked green arrow indicates exit block in HF hearts. **B**, Description of the project work flow. BGS indicates bovine growth serum; CT, crista terminalis; IAS, interatrial septum; IVC, inferior vena cava; LC-MS/MS, liquid chromatography with tandem mass spectrometry; miRNA, microRNA; RA, right atrium; SVC, superior vena cava; and TGFβ1, transforming growth factor β1.

injury responses including myocardial infarction[12,13] and chronic disease states. Hence, we aimed to develop an in-depth understanding of the phenotypic and molecular landscape of SAN fibroblasts in vitro and in situ together with intranodal ECM composition in nonfailing (non-HF) and HF human hearts, which could ultimately be used to target pathologic SAN fibrosis. We isolated and cultured human SAN and surrounding RA fibroblasts from human non-HF and HF hearts and subjected the same samples to quantitative proteomics and next-generation sequencing of the whole cellular transcriptome to generate, for the first time, a comprehensive atlas of protein expression, coding mRNA, and noncoding RNAs including long noncoding RNA (lncRNA) and microRNA (miRNA; Figure 1B).

METHODS

Detailed methods are provided in the Supplemental Methods in the Data Supplement. Proteomics data are publicly available at MassIVE (MSV000086692; https://doi.org/doi:10.25345/C5DN5P). RNA sequencing data have been deposited in National Center for Biotechnology Information's Gene Expression Omnibus[14] and are accessible with GSE164794 (https://www.ncbi.nlm.nih.gov/geo/query/acc.cgi?acc=GSE164794).

Human Cardiac Tissue Collection

Explanted failing hearts from transplant recipients (n=16; 54.9±2.6 years of age) with nonischemic or dilated cardiomyopathy with or without implantable cardiac defibrillator and left ventricular assist device and donor human hearts (non-HF; n=22; 48.7±3.1 years of age) without history of cardiac dysfunction and with intact SAN pacemaker complexes (Table I in the Data Supplement) were obtained from The Ohio State University Cardiac Transplant Team or LifeLine of Ohio Organ Procurement Organization, respectively, in accordance with the approved Ohio State University institutional review board with informed consent.

SAN and RA Fibroblast Isolation

Explanted human hearts were arrested and dissected in ice-cold cardioplegic solution (Figure 1B). Fibroblasts were isolated from the intramural SAN pacemaker compartment (<10×5×1.5 mm^3) and neighboring RA tissues by enzymatic digestion (Table II in the Data Supplement), cultured, passaged once, and synchronized in Dulbecco Modified Eagle Medium with 0.5% *bovine growth serum* for 24 hours. Subsequently, cells were treated with ±5 ng transforming growth factor β1 (TGFβ1) for 48 hours, after which the resulting pellet was used for RNA sequencing and proteomics.

Quantitative Proteomics and Next-Generation Sequencing

Mass spectrometry data were acquired from 3 µg peptides per sample. Database search of mass spectra from all samples (Excel File I in the Data Supplement) was performed with the OpenMS platform and X!Tandem search engine against a reviewed UniProt human proteome (downloaded September 4, 2019). RNA for next-generation sequencing was isolated from fibroblast cell pellets using the miRNeasy Kit (QIAGEN) according to the manufacturer's instructions (Excel File II in the Data Supplement). All data analyses were performed with R and various packages (full analysis pipelines and quality control are available in the Data Supplement).

Gene Ontology and KEGG Network Analyses

KEGG analysis (Kyoto Encyclopedia of Genes and Genomes) was performed with kegga and topKEGG functions in R for the top 20 terms. Data were filtered for significant enrichment only ($P<0.05$).

Statistical Analyses

Results are presented as mean±SEM in scatterplots with bars. The Shapiro-Wilk method was used to test normality of the group. Paired or unpaired Student *t* test (2-tailed) and 1- or 2-way analysis of variance (with Tukey test) were used to compare 2 or multiple groups where $P<0.05$ was considered statistically significant.

RESULTS

Fibrotic Content Increases in the HF SAN

Fibrotic content in the SAN pacemaker compartments and adjacent RA tissue was determined by quantifying fibrotic areas identified by Masson trichrome staining (non-HF=15, HF=13; Figure 2A). Analyses showed that percentage of dense fibrotic content was significantly higher across the SAN compartments versus RA in non-HF hearts (44.0±1.2 versus 24.7±1.7%; $P<0.0001$) and HF hearts (57.6±2.6 versus 34.4±1.3%; $P<0.0001$). Fibrotic content in SAN and RA in HF hearts was significantly higher than in non-HF hearts.

Interstitial ECM and Fibroblast Remodeling in the HF SAN

The first goal of our study was to determine ECM protein composition and characteristics of non-HF versus HF SAN fibroblasts in situ. Sections of non-HF and HF SAN were stained for collagen 1 and COL3A1 (collagen 3A1), CILP1 (cartilage intermediate layer protein 1), and POSTN (periostin), components of the ECM in pathologic remodeling and scars (Figure I and Table III in the Data Supplement). Collagen 1 to COL3A1 ratio was lower in SAN HF versus non-HF. CILP1 was higher (non-HF=1.0±0.2%; HF=3.7%±0.4% [$P<0.0001$]) in HF SAN; ratios of CILP1 to collagen 1 and COL3A1 were higher in HF compared with non-HF SAN (Figure 2B). Interstitial POSTN expression in the SAN pacemaker compartments was found only in HF SAN; it was negligible in non-HF (Figure 2C). Cryosections from non-HF and HF SAN were immunostained with α-actinin,

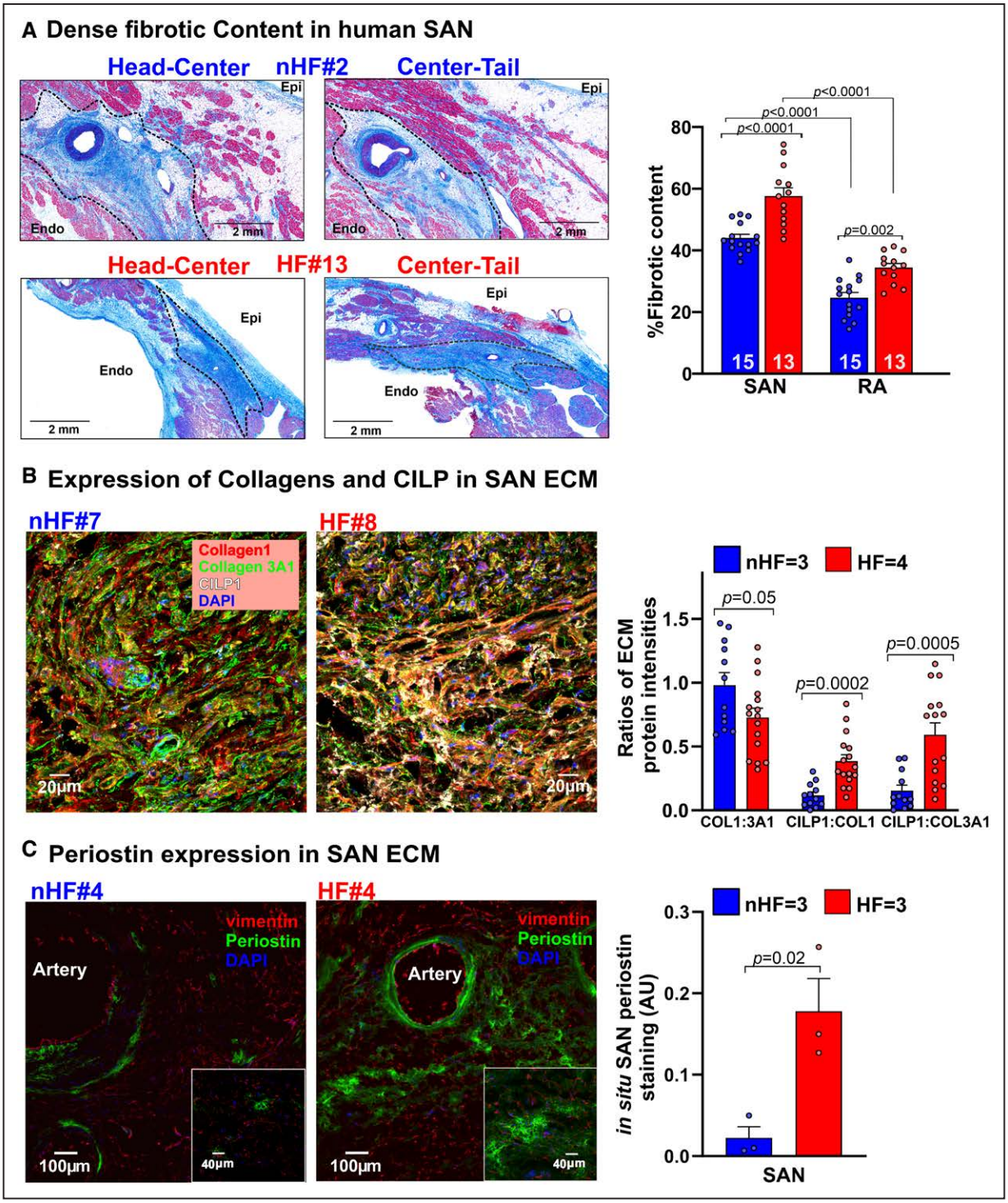

Figure 2. Quantification of dense connective tissue and composition of extracellular matrix (ECM) in human sinoatrial node (SAN). **A**, **Left**, Representative images show dense connective tissue and fibrosis (blue) identified in Masson trichrome–stained paraffin-embedded human nonfailing (no heart failure [nHF]; n=15) and failing (heart failure [HF]; n=13) SAN sections, respectively. **Right**, Quantification of dense connective tissue from sections of SAN head, center, and tail compartments. Each dot is an average of at least 3 measurements per SAN and right atrium (RA). **B**, **Left**, Representative images of ECM proteins COL1 (collagen 1; red), COL3A1 (collagen 3A1; green), and CILP1 (cartilage intermediate layer protein 1; white) staining in nHF and HF SAN cryosections (see also Figure IA in the Data Supplement). **Right**, Summary data of their ratios (nHF [n=3] and HF [n=4]; each dot is an average of measurements from 4 fields of view per SAN). **C**, **Left**, nHF and HF SAN cryosections stained with vimentin (red) and POSTN (periostin; green). Cell nuclei were stained with DAPI (4′,6-diamidino-2-phenylindole; blue). **Right**, Summary data of POSTN staining density (nHF [n=3] and HF [n=3]; each dot represents measurement from each SAN). All data were analyzed with analysis of variance (2- or multiple-group comparison, as applicable) and expressed as mean±SEM ($P<0.05$). CT indicates crista terminalis; Endo, endocardial; Epi, epicardial; and IAS, interatrial septum.

vimentin, and CD31 (cluster of differentiation 31) antibodies to identify cardiomyocytes, fibroblasts, and endothelial cells, respectively (Figure 3A). A percentage of vimentin$^+$/CD31$^-$ cells were quantified as fibroblasts, which was comparable between non-HF (66±6%) and HF (61±5%) SAN sections (P=0.18). However, vimen-

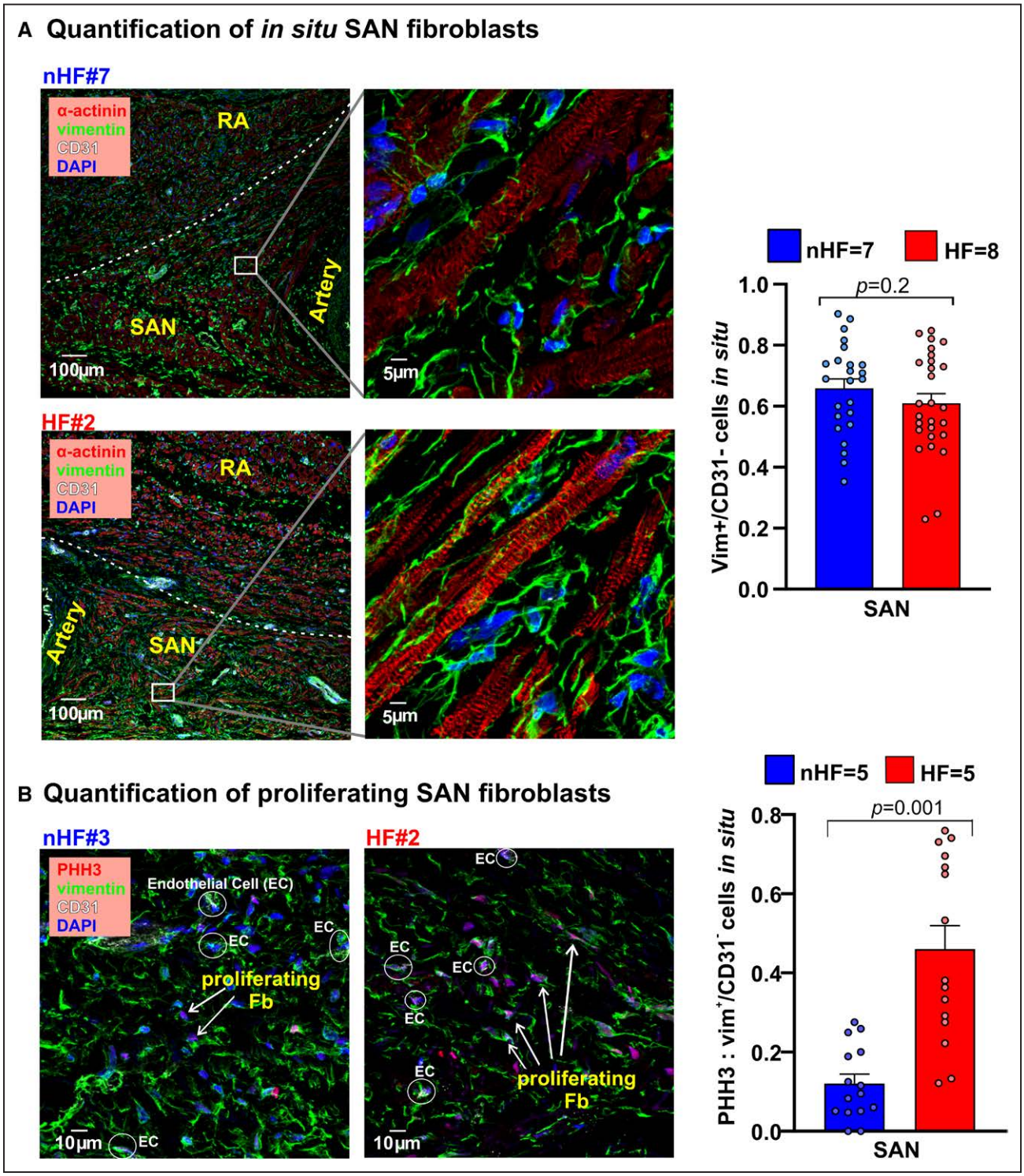

Figure 3. Composition of fibroblasts in non–heart failure (nHF) and heart failure (HF) human sinoatrial node (SAN). **A**, **Left**, Fibroblasts in the nonfailing (n=7) and failing (n=8) SAN stained in cryosections with vimentin (green), cardiomyocytes with α-actinin (red), and DAPI (4′,6-diamidino-2-phenylindole; blue). **Right**, Summary data of vimentin-positive cells relative to all cells. Each dot is an average of measurements from 3 to 4 fields of view per SAN. **B**, **Left**, Sections from nHF and HF SAN stained for vimentin (green), PHH3 (phosphorylated histone 3; red), CD31 (cluster of differentiation 31; white), and DAPI (blue). **Right**, Summary of proliferating fibroblasts quantified as a ratio of PHH3-positive cells to vimentin$^+$/CD31$^-$ cells (nHF [n=5] and HF [n=5]; each dot is an average of measurements from 3 fields of view per SAN). All data were analyzed with analysis of variance and expressed as mean±SEM (P<0.05). RA indicates right atrium.

tin$^+$/CD31$^-$ cells positive for the proliferation marker PHH3 (phosphorylated histone H3) were higher in HF compared with non-HF SAN (0.46±0.05 versus 0.12±0.02; P=0.001; Figure 3B).

In Situ, Myofibroblasts Are Present in the HF SAN but Not in Non-HF SAN

Next, we examined the composition of fibroblasts and myofibroblasts in situ to determine inherent qualitative differences between the SAN and RA, which could correlate with their fibrotic content. Cryosections were stained for vimentin, CD31, and α-smooth muscle actin (αSMA; n=3; 3 fields of view/heart) to identify differentiated myofibroblasts in the SAN (Figure 4A and Figure II in the Data Supplement). Thirty-nine percent αSMA$^+$/vimentin$^+$/CD31$^-$ myofibroblasts were found in HF SANs relative to αSMA$^-$/vimentin$^+$/CD31$^-$ fibroblasts, but no definitive myofibroblasts were found in non-HF SAN sections.

In Vitro, HF Fibroblasts Show Robust Myofibroblast Differentiation and Fibronectin Secretion

We studied the composition of non-HF and HF SAN and RA cultured fibroblasts ± TGFβ1. TGFβ1 was used to activate myofibroblast transdifferentiation in these populations and determine whether it would be increased in HF-derived cells, because we predicted that SAN and RA fibroblasts from HF hearts would already be activated in situ compared with non-HF hearts. We also hypothesized that SAN fibroblasts from non-HF hearts would have an inherently higher propensity to transdifferentiate than corresponding RA cells (Figure 4B). In line with this rationale, αSMA-positive myofibroblasts were found in untreated non-HF SAN and HF SAN and RA fibroblast cultures. TGFβ1 treatment significantly increased the number of myofibroblasts in non-HF and HF SAN and non-HF RA (Figure 4C). Fibronectin staining was higher in untreated HF versus non-HF SAN fibroblast cultures; it increased after TGFβ1 treatment only in non-HF SAN fibroblast cultures. Untreated HF SAN cultures also showed higher fibronectin staining compared with non-HF SAN cells.

Whole Transcriptomic Profiles in SAN and RA Cultured Fibroblasts

Our next goal was to evaluate and quantify the global expression of all fibroblast-specific transcripts in the SAN and RA cultured fibroblast groups. Enrichment of fibroblasts excluding other cell types (endothelial cells and macrophages) was confirmed by immunostaining for all samples. Immunostaining with cyclins A2, D1, and PHH3 antibodies confirmed that fibroblasts from both nonfailing and failing cultures are not actively cycling or proliferating (Figure III in the Data Supplement). Whole transcriptome of SAN and RA samples was sequenced for 40 samples from 5 non-HF and 5 HF hearts (samples from 3 hearts [2 non-HF and 1 HF] were removed from the sequencing and proteomics analyses because of low protein spectral counts from complementary proteomics analyses; Excel File I in the Data Supplement). Genes expressed lower than the minimum count per million of 0.59 (equivalent to 10 counts) in at least 3 samples in 1 group were filtered, and the resulting sequenced reads were normalized with trimmed mean of M values. Across the 8 test groups, averages of total counts revealed that majority of the genes detected were protein coding mRNAs (14 415 genes [63%]); then, in decreasing prevalence, lncRNA (5876 [26%]), miscellaneous RNA (1254 [5%]), miRNA (677 [3%]), and other types of RNA (577 [3%]; Figure 5A and Table IV in the Data Supplement).

Protein coding mRNA and lncRNA were further analyzed to determine their distinctive patterns in SAN versus RA fibroblasts; Venn diagrams in Figure 5B represent analyses of mRNA counts in SAN and RA fibroblasts from non-HF and HF hearts and reveal different patterns of unique versus commonly expressed mRNAs between non-HF SAN versus RA and HF SAN versus RA. Unique and common mRNAs were detected after TGFβ1 treatment.

Fibroblast-Specific SAN mRNA Profiles

In addition to differences in mRNA profiles across the groups (Figures IV–VIII in the Data Supplement), we first examined the expression of several mRNAs associated with fibrosis and with the TGFβ pathway in SAN and RA fibroblasts (Figure 5C). Scaled expression levels (z scores of count per million) of these selected profibrotic genes across the data sets showed differing patterns between SAN and RA samples from non-HF hearts, indicating specific differences in these cultured fibroblasts and TGFβ1-induced myofibroblast samples (Figure 5C). mRNAs including *Smad2/3*, *Tgfbr3*, and other profibrotic proteins, including fibulin3 (*Fbln3*), sulfatase1 (*Sulf1*), keratin8 (*Krt8*), tenascin X (*Tnxb*), laminin2 (*Lama2*), and Cx45 (*Gjc1*), decreased in both SAN non-HF and HF myofibroblasts after TGFβ1 treatment. Similarly, mRNA counts of collagens (*Col3A1*, *Col1A2*), elastin (*Eln*), LTBP2 (latent transforming growth factor binding protein; *Ltbp2*), *Postn*, cartilage oligomeric matrix protein (*Comp*), *Cilp1*, and fibrillin 1 (*Fbn1*) were increased in TGFβ1-treated non-HF and HF SAN fibroblasts. These trends indicate similar transcriptional activation patterns in non-HF and HF SAN fibroblasts. In contrast, smooth muscle actin (*Acta2*) and Lysl oxidase (*Lox)* were increased only in TGFβ1 HF SAN fibroblasts, supporting increased myofibroblastic differentiation in the setting

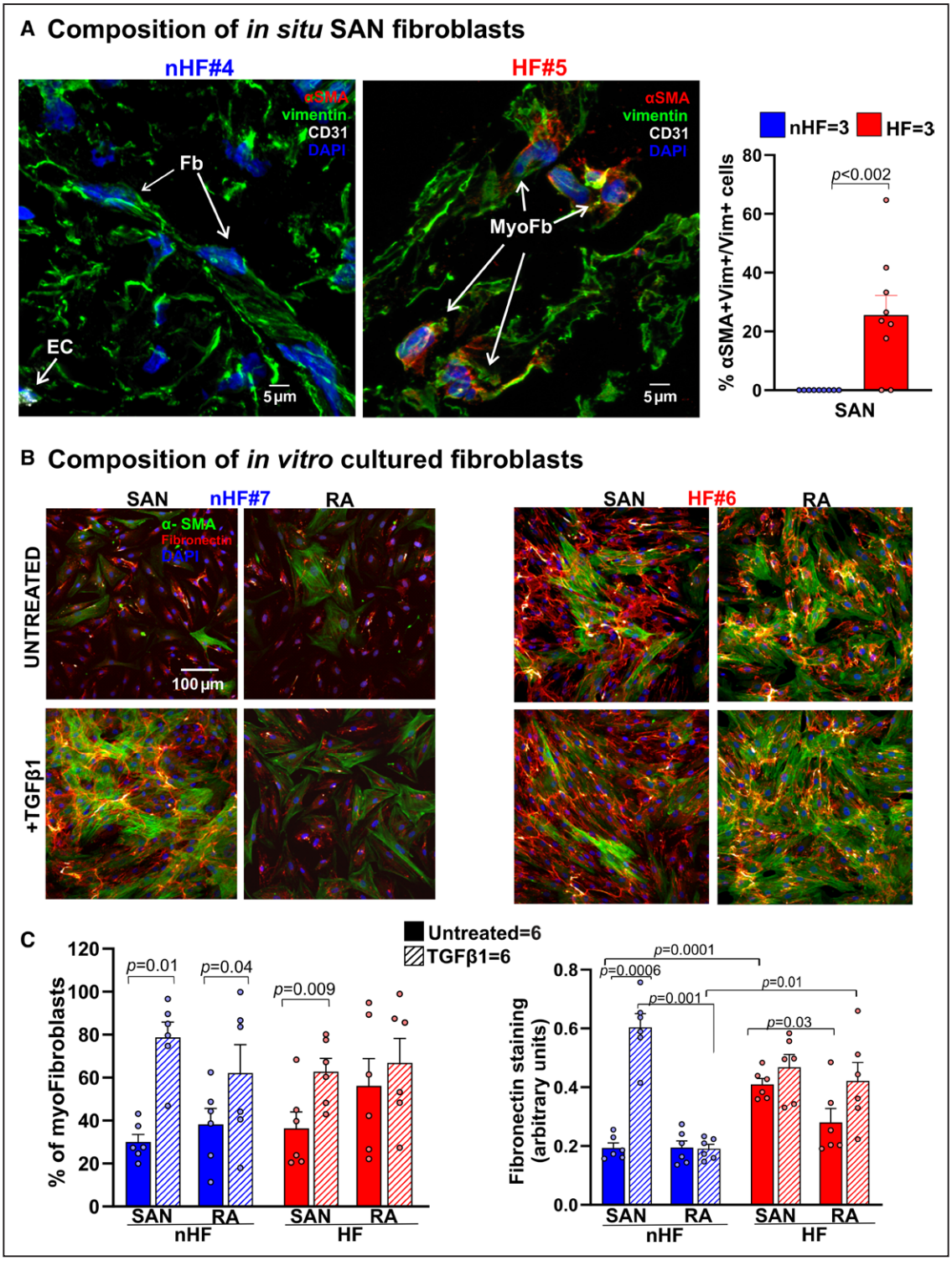

Figure 4. Composition of in situ and in vitro non–heart failure (nHF) and heart failure (HF) human sinoatrial node (SAN) fibroblasts.

A, Representative images of nonfailing (nHF; n=3) and failing (HF; n=3) human SAN cryosections stained for αSMA (α-smooth muscle actin; red), vimentin (vim; green), and CD31 (cluster of differentiation 31; white) identifying vimentin$^+$/αSMA$^-$ fibroblasts (Fb), vimentin$^+$/αSMA$^+$ myofibroblasts (myoFb), and CD31$^+$/αSMA$^+$ endothelial cells (EC). Each dot is an average of measurements from 3 fields of view per SAN. **B**, Representative images of isolated SAN and right atrium (RA) fibroblasts from nHF or HF hearts cultured for 48 hours ± transforming growth factor β1 (TGFβ1). Cells were stained with αSMA (green) and fibronectin (red). **C**, Summary data of myofibroblast percentages in the cultures and quantification of fibronectin staining (nHF [n=6] and HF [n=6]; each dot is a measurement from SAN/RA ± TGFβ1 cultures). Cell nuclei were stained with DAPI (4′,6-diamidino-2-phenylindole; blue). Data were analyzed with analysis of variance (2- or multiple-group comparison, as applicable) and expressed as mean±SEM ($P<0.05$).

ORIGINAL RESEARCH ARTICLE

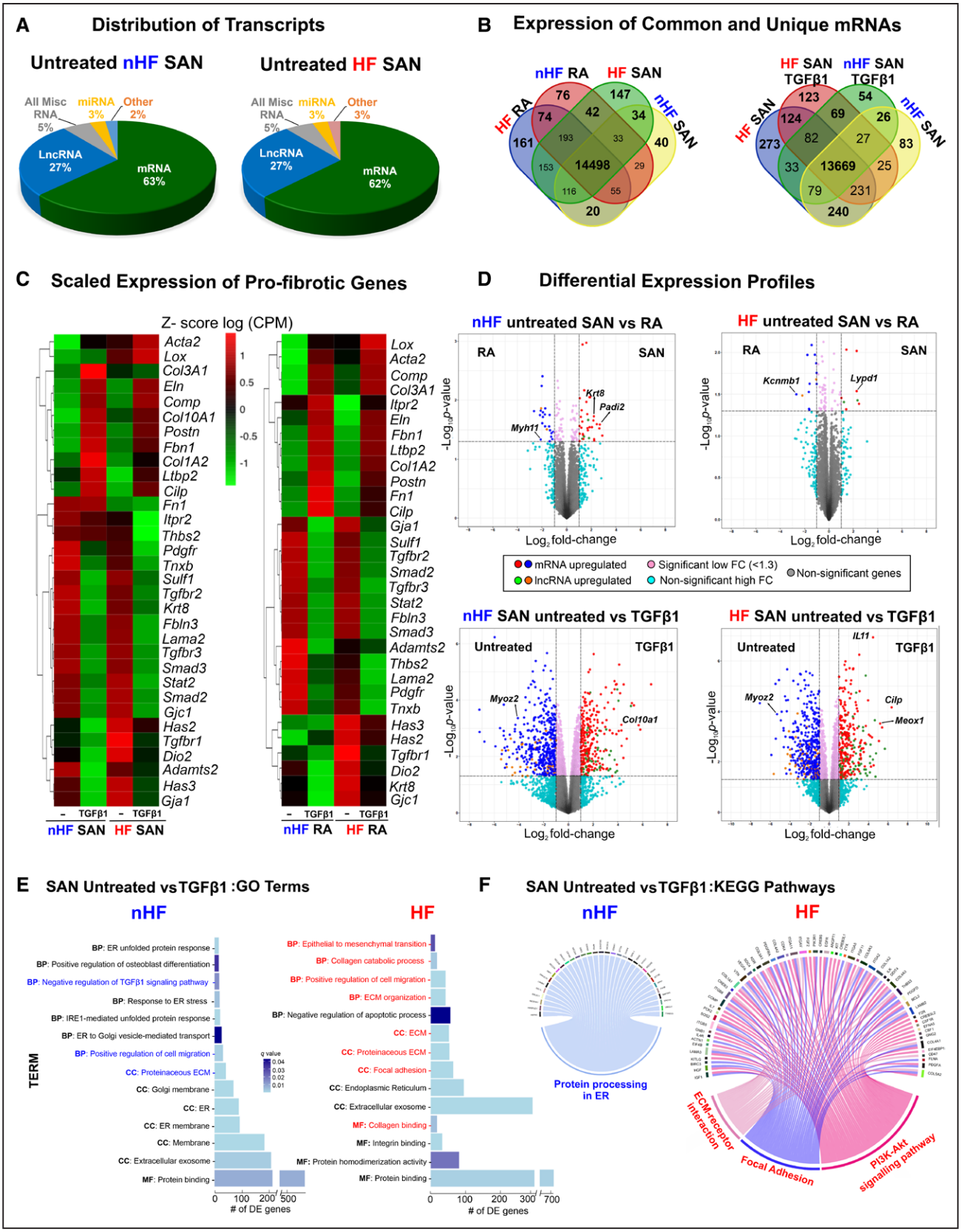

Figure 5. Whole transcriptomic profiles of human sinoatrial node (SAN) fibroblasts.
A, Distribution of major coding and noncoding transcript groups detected across untreated nonfailing (no heart failure [nHF]) and failing (heart failure [HF]) SAN fibroblasts. **B**, Venn diagrams show unique and shared mRNAs between SAN comparison groups. **C**, Heatmaps show scaled expression levels of selected profibrotic genes in nHF and HF SAN vs right atrium (RA) ± transforming growth factor β1 (TGFβ1) groups. (*Continued*)

Figure 5 Continued. D, Volcano plots of mRNAs and long noncoding RNAs (lncRNAs) differentially expressed between groups shown at $P<0.05$ and $\log_2$ fold change (FC)>1.3. **E**, Differentially expressed (DE) genes ($q<0.05$) enriched within 3 gene ontology (GO) analysis terms in nHF and HF untreated vs TGFβ1 fibroblasts (selected terms are presented). **F**, Circos plots show differentially expressed genes ($P<0.05$) associated with Kyoto Encyclopedia of Genes and Genomes (KEGG) pathways in nHF and HF untreated vs TGFβ1 SAN fibroblasts (nHF=3; HF=4). Magnified images of GO and KEGG plots are presented in Figure IX in the Data Supplement. Akt indicates protein kinase B; BP, biological process; CC, cellular component; CPM, count per million; ECM, extracellular matrix; ER, endoplasmic reticulum; IRE1, inositol-requiring transmembrane kinase/endonuclease; MF, molecular function; miRNA, microRNA; Misc, miscellaneous; mRNA, coding messenger RNA; and PI3K, phosphoinositide 3-kinase.

of HF. Similarly, hyaluronan synthase 3 (*Has3*) and Cx43 (*Gja1*) transcripts were detected in untreated non-HF and HF SAN fibroblasts, but decreased in TGFβ1-treated fibroblasts.

Comparing non-HF SAN and RA gene expressions, 20 mRNAs were found upregulated ($P<0.05$ and log fold change>1.3) in SAN fibroblasts, including keratin8 (*Krt8*), and 14 different mRNAs were upregulated in RA fibroblasts, including myosin heavy chain 11 (*Myh11*; Figure 5D, top left; Excel File III in the Data Supplement). SAN fibroblasts from HF hearts showed 13 mRNA upregulated in SAN fibroblasts, including Ly6/Plaur domain-containing 1 (*Lypd1*) and potassium channel tetramerization domain containing 8 (*Kctd8*), and 36 upregulated in the RA fibroblasts, including the large-conductance potassium channel b subunit (*Kcnmb1*; Figure 5D, top right; Excel File IV in the Data Supplement). Differential expression analyses comparing the activated response of untreated non-HF SAN fibroblasts with TGFβ1 showed 241 mRNAs to be different between the groups ($P<0.05$, log fold change>1.3; Figure 5D, bottom left; Excel File V in the Data Supplement). Between untreated HF SAN versus TGFβ1-treated SAN fibroblasts, 124 were upregulated in the untreated group, including myozenin 2 (*Myoz2*; Figure 5D, bottom right; Excel File VI in the Data Supplement), and 56 in TGFβ1-treated HF SAN fibroblasts, including *Cilp1* and mesenchyme homeobox 1 (*Meox*1).

Gene ontology analyses of differentially expressed mRNAs in treated versus untreated non-HF SAN revealed 16 significantly enriched categories ($q<0.05$), including endoplasmic reticulum–related functions, proteinaceous ECM, and positive regulation of cell migration. Differentially expressed mRNA in treated versus untreated HF SAN were statistically enriched in 21 categories, including epithelial to mesenchymal transition, focal adhesion, collagen, and ECM matrix organization (Figure 5E and Excel File VII in the Data Supplement). Analyses with the KEGG database showed differentially expressed mRNAs in TGFβ1-treated non-HF SAN fibroblasts in 1 signaling pathway related to protein processing in endoplasmic reticulum (Figure IX in the Data Supplement). ECM–receptor interaction, focal adhesion, and PI3K (phosphoinositide 3-kinase)–Akt (protein kinase B) signaling pathways were enriched in HF groups compared with non-HF SAN (Figure 5F).

Fibroblast-Specific SAN LncRNA Profiles

Similar to mRNA profiles, several lncRNAs were also found to be differentially expressed between the SAN and RA groups (Figure 5D). We found several annotated but uncharacterized lncRNAs to be differentially expressed in these groups. Moreover, multiple common and unique lncRNAs were detected in all groups (Figure 6A). We also compared scaled expression of lncRNAs previously associated with fibrosis or cardiac diseases[12,15–17] (Figure 6B). Although we did not find significant differences, scaled expression of z scores showed that *Malat1* was higher in untreated non-HF SAN versus TGFβ1, whereas it increased only after TGFβ1 in RA relative to untreated; TGFβ1 increased *Neat1* only in non-HF RA but not in the SAN.

Fibroblast-Specific SAN miRNA Profiles

miRNA quantitation identified >12 million reads/sample. In non-HF and HF hearts, both common and unique miRNAs were detected in RA and SAN fibroblasts (Figures X and XI in the Data Supplement). Differential expression analyses revealed that 4 miRNAs (miRNA-615-3p, miRNA-10b-3p, miRNA-10b-5p, and miRNA-1292-5p) were upregulated in the non-HF SAN and 51 miRNAs in the non-HF RA (Figure 6C, top left). In HF hearts, 41 miRNAs were highly expressed in the SAN and 41 miRNAs were highly expressed in the RA (Figure 6C, top right). When comparing differential expression of miRNAs between SAN fibroblasts in non-HF versus HF hearts, a different pattern was found, with 19 differentially expressed miRNAs: 13 miRNAs were upregulated in the HF SAN fibroblasts and 6 in non-HF fibroblasts. In contrast, 13 miRNAs were upregulated in RA HF fibroblasts; only 3 miRNAs were upregulated in non-HF fibroblasts (Figure XI in the Data Supplement).

miRNA profiles showed different patterns between non-HF and HF SAN fibroblasts in response to TGFβ1. Only miRNA-1306-5p was upregulated in untreated non-HF SAN fibroblasts, but 25 miRNAs were found upregulated in TGFβ1-treated non-HF SAN fibroblasts (Figure 6C, bottom left). On the other hand, in HF SAN, 31 miRNAs were upregulated after TGFβ1 compared with 20 miRNAs upregulated in untreated fibroblasts (Figure 6C, bottom right). Hierarchical cluster analyses ($P<0.05$; Figure 6D and Excel File VIII in the Data Supplement) also revealed that both HF and TGFβ1 affected

ORIGINAL RESEARCH ARTICLE

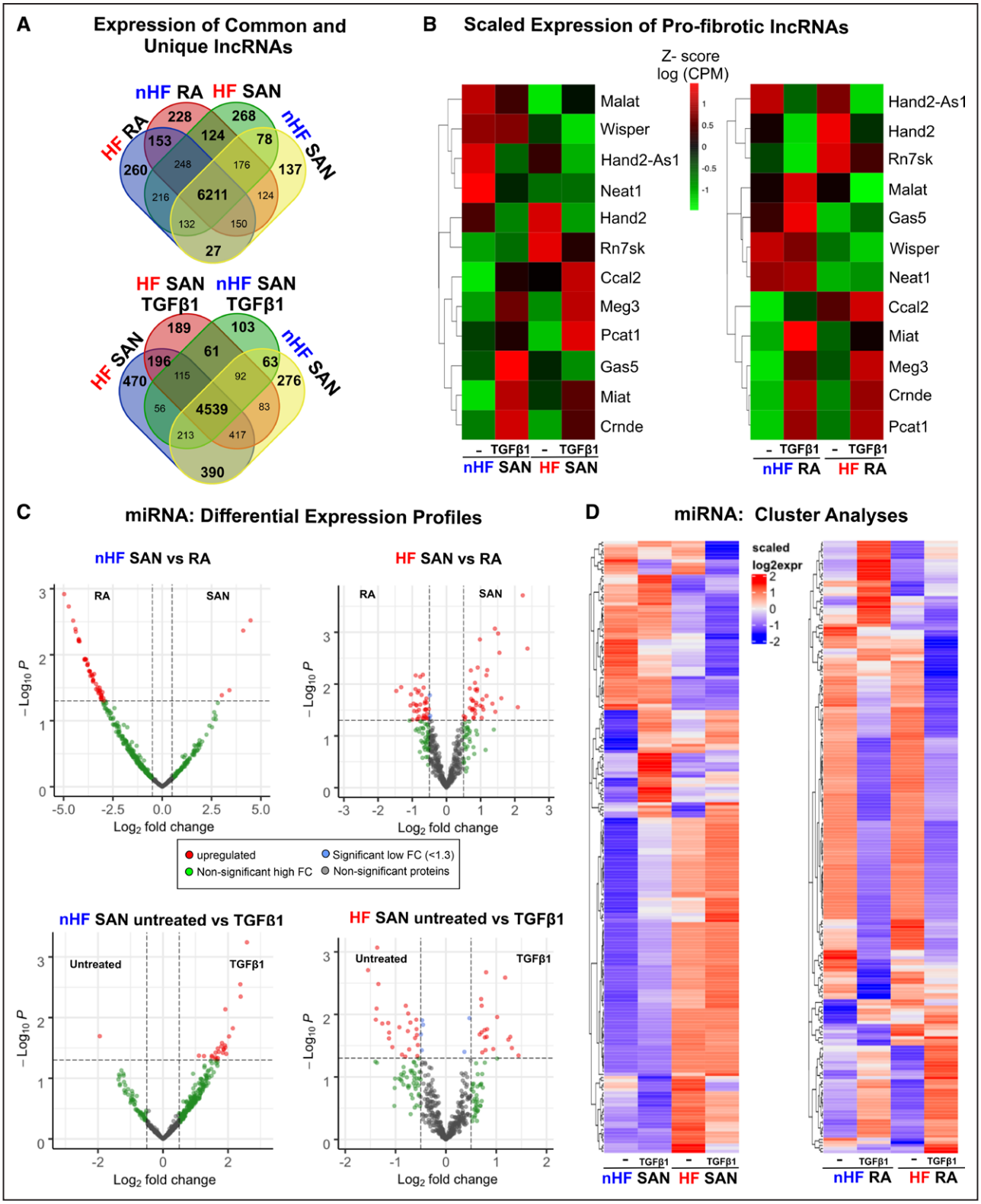

Figure 6. Differential expression of long noncoding RNAs (lncRNA) and microRNAs (miRNAs).
A, Distribution of lncRNAs across untreated nonfailing (no heart failure [nHF]) and failing (heart failure [HF]) untreated and + transforming growth factor β1 (TGFβ1) sinoatrial node (SAN) fibroblast comparison groups. **B**, Heatmaps show scaled expression levels of selected profibrotic lncRNAs in nHF and HF SAN vs right atrium (RA) ± TGFβ1 groups. **C**, Volcano plots of miRNAs differentially expressed between shown groups at $P<0.05$ and $\log_2$ fold change (FC)>1.3. **D**, Heatmaps show scaled expression levels of miRNAs differentially expressed ($P<0.05$) in nHF and HF SAN vs RA ± TGFβ1 groups (nHF=3; HF=4). CPM indicates count per million.

expression patterns of miRNAs differently in the SAN and RA fibroblasts.

Predicted Interactions and Networks of miRNAs and Their Target mRNAs

Ingenuity pathway analyses of interactions between significantly different miRNAs and mRNAs among non-HF SAN versus HF SAN untreated fibroblasts revealed 33 interactions, of which 9 miRNAs are inverse, suggesting putative miRNA mediated regulation of mRNA targets (Figure 7A and Table V in the Data Supplement). Among the differentially expressed miRNAs between non-HF SAN untreated versus TGFβ1, 47 showed interactions with multiple differentially expressed mRNAs; 22 interactions were inversely paired in expression. Twelve differentially expressed miRNAs were predicted to interact with selected ECM genes, of which 10 were inversely paired (Figure 7B and Table VI in the Data Supplement). Among miRNAs differentially expressed between HF SAN untreated versus TGFβ1, 51 miRNAs were predicted to interact with selected ECM-related mRNAs, of which 26 were inversely paired (Figure 7C and Table VII in the Data Supplement).

Proteomic Profiles in SAN and RA Fibroblasts

Next, we examined the proteomic profiles in the same cultured fibroblast populations. Data from liquid chromatography with tandem mass spectrometry studies (Table VIII in the Data Supplement and Figures XII–XV) were analyzed for unique and common proteins among the groups (Figure 8A). Comparing protein expression in SAN fibroblasts, 176 proteins were unique to untreated non-HF and 89 to untreated HF group, indicating a distinctive protein composition between untreated non-HF and HF SAN fibroblasts, with 51 proteins unique to both groups (Figure 8A, middle Venn diagram). Similarly, after TGFβ1 treatment, non-HF and HF SAN groups showed 36 and 192 proteins, respectively, that were unique to each group; 42 were shared.

Comparing scaled expression patterns in SAN versus RA non-HF untreated fibroblasts of the selected proteins associated with fibrosis and ECM secretion, SAN fibroblasts demonstrated higher levels of COL3A1, filamin A, reticulin1, STAT2 (signal transducer and activator of transcription 2), and focal adhesion proteins annexin6, TLN1 (talin1), and vinculin (Figure 8B). After TGFβ1 treatment, SAN and RA non-HF fibroblasts showed similar changes in expression of several proteins; COL3A1 remained higher in SAN non-HF TGFβ1 fibroblasts. SAN versus RA HF untreated cells showed lower levels of COL3A1, caldesmon1, fibulin3, and filamin A/B. TGFβ1 treatment similarly increased annexin6, collagen 1A2, filamin B, LTBP2, POSTN, RET1 (retinol binding protein), SYNE1 (nesprin), tensin1, and vinculin in both SAN and RA HF fibroblasts. COL3A1, caldesmon1, fibrillin1, STAT1 (signal transducer and activator of transcription 1), STAT2, and TLN1 were lower in HF SAN after TGFβ1 compared with RA.

We next examined the differential expression of proteins in these groups. An average of 2867 proteins were detected across the 8 comparison groups (Table VIII in the Data Supplement) and differentially expressed proteins were determined significant ($P<0.05$ and log fold change>1.3; Figure 8C). Proteins including laminin and smooth muscle myosin heavy chain 11 were upregulated in untreated non-HF RA fibroblasts whereas STAT2, VAV2, and ITPR2 (inositol 1,4,5-trisphosphate receptor) were upregulated in untreated non-HF SAN fibroblasts. In contrast, a different set of proteins was upregulated in HF SAN and RA fibroblasts. TGFβ1 treatment increased POSTN, LTBP2, collagen 5, collagen A1, and collagen 2 in non-HF SAN cells, whereas SYNE1, RET1, CADH2 (cadherin2), and ITA4 (integrin-α4) were increased in HF SAN cells.

Gene ontology analyses of differentially expressed proteins revealed 20 significantly enriched categories in non-HF SAN untreated versus TGFβ1 related to ECM, collagen fibril organization, collagen trimers, and epidermal growth factor receptor activation, whereas 20 categories, including cytoplasmic functions, actin cytoskeleton, stress fiber, ECM constituents, and biosynthetic pathways, were enriched in HF (Figure 8D and Figure XVI in the Data Supplement). Analysis with KEGG database identified 10 highly enriched pathways between untreated and TGFβ1 non-HF SAN fibroblasts including JAK (Janus kinase)–STAT signaling and 17 signaling pathways including ECM–receptor interaction, focal adhesion, arrhythmogenic right ventricular cardiomyopathy, and metabolic pathways among differentially expressed proteins from untreated versus TGFβ1 HF SAN fibroblasts (Figure 8E and Excel File IX in the Data Supplement). Overall, proteomic signatures in SAN and RA fibroblasts were uniquely affected by HF or TGFβ1 treatment.

DISCUSSION

In recent years, extensive research has demonstrated cardiac fibroblasts to be equally important as cardiomyocytes in their effect on structure and function of the healthy and diseased heart.[18,19] The human SAN is designed to serve as the leading pacemaker, which persistently generates and conducts electric activity to the atria. For these functions, the specialized pacemaker cardiomyocytes require the dense fibrotic fibers that form a structural lattice and define conduction pathways into the atria.[1] Pathologic remodeling of ECM composition and fibrosis preferentially increases in the SAN during HF (Figure 2A), which can contribute to automaticity and conduction abnormalities found in diseased hearts.[9–11]

Figure 7. Predicted interactions and networks between microRNAs (miRNAs) and profibrotic mRNAs in fibroblasts.
Ingenuity pathway analyses predicted interactions and networks between miRNAs ($P<0.05$; green) and selected profibrotic mRNAs (red) in (**A**) sinoatrial node (SAN) untreated non–heart failure (nHF) vs heart failure (HF); (**B**) SAN nHF untreated vs transforming growth factor β1 (TGFβ1) fibroblasts; and (**C**) SAN HF untreated vs TGFβ1 fibroblasts (nHF=3; HF=4). Direction of arrows indicates upregulation or downregulation of the respective transcripts. Lines indicate predicted interactions between networks.

We found that while CILP1[20] increases, COL3A1 expression decreases, leading to higher ratios of CILP1 to collagen 1 and COL3A1 in HF versus non-HF SAN (Figure 2B). This remodeling of ECM protein composition may promote less flexible and stiffer SAN ECM. POSTN, associated with pathologic fibrosis and myocardial scars, cell-to-matrix signaling, and epithelial–mesenchymal transition,[21,22] was negligible in the human non-HF SAN but detected in all HF SANs studied, and appeared as concentrated islands within the ECM (Figure 2C). Such

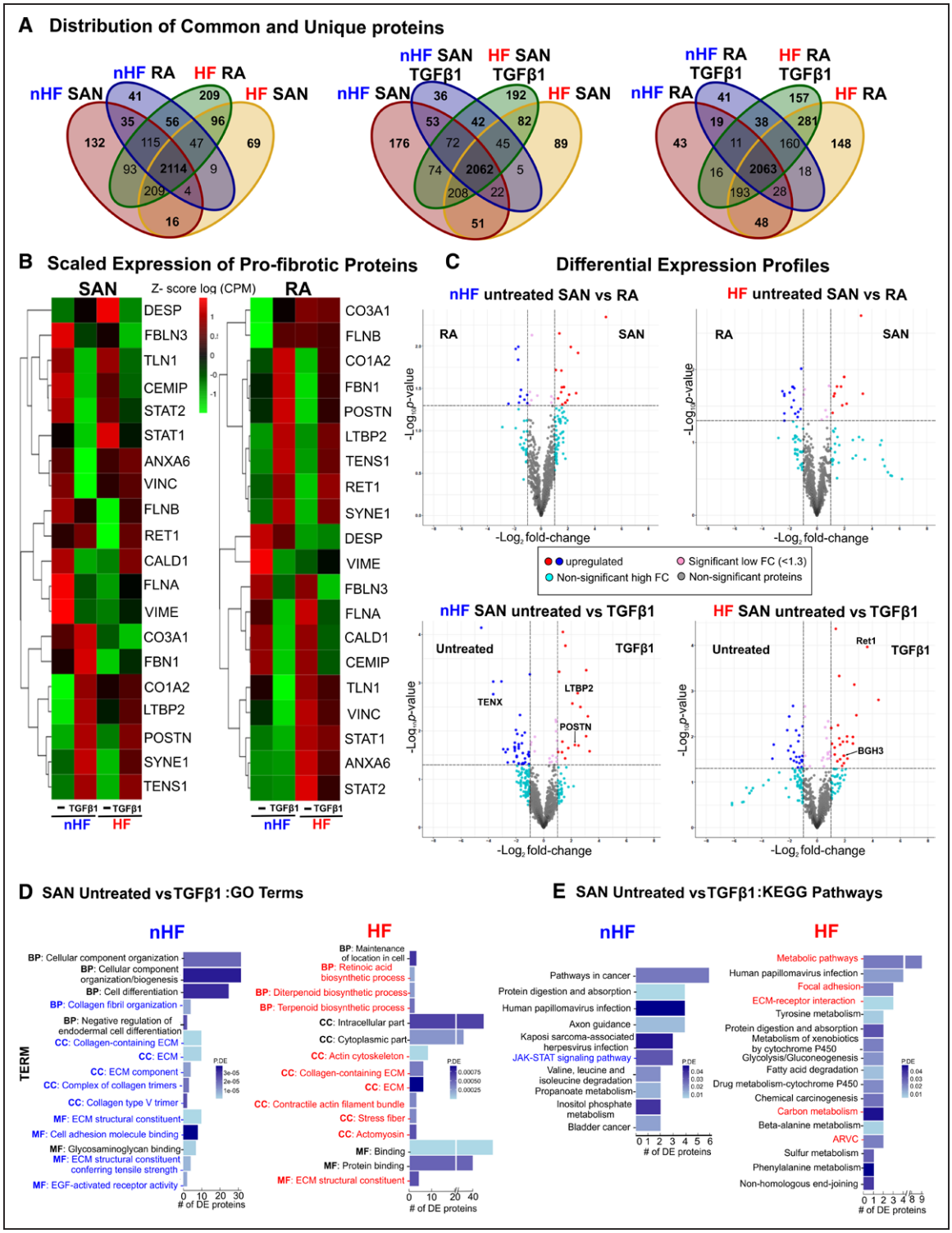

Figure 8. Differential proteomic profiles of human sinoatrial node (SAN) fibroblasts.
A, Venn diagrams show unique and shared proteins among non–heart failure (nHF) and heart failure (HF) SAN vs right atrium (RA) (**left**), SAN nHF vs HF ± transforming growth factor β1 (TGFβ1) (**middle**), and RA nHF vs HF ± TGFβ1 (**right**) fibroblast populations. **B**, Heatmaps show scaled expression levels (counts per million [CPM]) of selected profibrotic proteins in nonfailing and failing SAN vs RA ± TGFβ1 groups. **C**, Volcano plots of proteins differentially expressed at $P<0.05$ and $\log_2$ fold change (FC)>1.3 are in red or blue. **D**, Differentially expressed proteins ($P<0.05$) enriched within 3 gene ontology (GO) analyses terms in nHF and HF untreated vs TGFβ1 fibroblasts (selected terms are presented). **E**, Kyoto Encyclopedia of Genes and Genomes (KEGG) pathways associated with differentially expressed (DE) proteins ($P<0.05$) in nHF and HF untreated vs TGFβ1 SAN fibroblasts (nHF=3; HF=4). Magnified images of GO and KEGG plots are presented in Figure XVI in the Data Supplement. ARVC indicates arrhythmogenic right ventricular cardiomyopathy; BP, biological process; CC, cellular component; ECM, extracellular matrix; EGF, epidermal growth factor; and MF, molecular function.

fibrotic islands/strands can create electric barriers interrupting mutual entrainment between pacemaker cardiomyocyte clusters and conduction pathways between SAN and RA leading to tachycardia–bradycardia, chronotropic incompetence, and SAN conduction blocks often associated with HF.[8,11]

Little is known about SAN fibroblasts, mainly because of the primary focus on SAN pacemaker cardiomyocytes as drivers of SAN function, with no emphasis on the fibrotic framework's role in efficient automaticity and conduction.[23] A single report previously showed that SAN fibroblasts form a network in a rabbit model.[24] We found similar numbers of fibroblasts in non-HF and HF human SAN studied, indicating that disease may not affect overall SAN fibroblast numbers (Figure 3A). However, the number of proliferative PHH3$^+$/vimentin$^+$/CD31$^-$ fibroblasts were higher in HF SAN (Figure 3B) and, in contrast to previous findings that reported higher myofibroblasts in human HF ventricle,[25] vimentin$^+$/αSMA$^+$/CD31$^-$ myofibroblasts were present only in the HF SAN (Figure 4A).

In contrast to in situ findings, in vitro cultured SAN and RA fibroblasts revealed robust myofibroblastic differentiation and fibronectin secretion when treated with TGFβ1 (Figure 4B and 4C). Our quantitative analyses of proteotranscriptomes of the same samples of cultured fibroblast populations showed similarities in the overall expression patterns of selected profibrotic mRNAs after TGFβ1 treatment between non-HF and HF SAN fibroblasts, indicating common signaling pathways and mechanisms between them (Figure 5). It is possible that these common profibrotic mRNAs are not additionally affected by HF. Exceptions were *Lox*, associated with collagen crosslinking, and *αSMA*, which were upregulated in HF SAN TGFβ1-induced myofibroblasts, which could promote denser and stiffer ECM properties and an enhanced contractile phenotype, respectively. We also found higher scaled expression of *Comp* and *Cilp1*, markers of matrifibrocytes associated with mature scars,[26] in TGFβ1-treated non-HF and HF SAN fibroblasts, implicating a role for similar specialized myofibroblasts, in addition to the classical αSMA$^+$ myofibroblasts, in the accumulation of dense fibrotic SAN tissue.

We found a potential role for inflammation in modulating SAN fibroblasts implicated with upregulation of profibrotic cytokine *IL11* mRNA after TGFβ1 treatment in both non-HF and HF SAN and RA fibroblasts (Figure 5D). In human RA fibroblasts, cytokine IL11 was recently shown to play an important role in cardiovascular fibrosis,[27] suggesting similar profibroinflammatory roles in the HF SAN. *Myoz2* encoding calsarcin1, previously identified in slow twitch skeletal muscle and enriched in cardiomyocytes,[28,29] increased in untreated non-HF and HF SAN and RA fibroblasts, suggesting that it is also expressed in fibroblasts and not restricted only to myocytes. Because *Myoz2* mutations have been shown to cause human cardiomyopathies, it would be important to determine whether these mutations affect nonmyocyte cells as well.[30] Similarly, transcription factor *Meox1*, recently shown to play a central regulatory role in stress-induced myofibroblast activation,[31] was higher in non-HF and HF SAN TGFβ1 fibroblasts relative to untreated fibroblasts.

Gene ontology and KEGG analyses in SAN HF groups also identified enrichment of genes in pathways of ECM–receptor interaction, focal adhesion, and the PI3K-Akt signaling pathway, which is associated with switching TGFβ1 signaling from apoptosis to epithelial–mesenchymal transition with increasing ECM stiffness[32] (Figure 5E and 5F). These gene expression patterns and enriched pathways suggest mature myofibroblasts and increased myofibroblastic differentiation in HF, which could lead to higher levels of fibrosis in HF SAN.

Studies have identified several lncRNAs in the heart and fibroblasts from cardiac tissues, but few data exist to document their relevance in the human heart.[16,33–36] This study is the first to document lncRNAs specific to human SAN fibroblasts. Our study identified several unique and common lncRNAs in all groups of fibroblasts studied (Figures 5D and 6A). LncRNAs *Malat1*[17] and *Gas5*,[37] previously shown to activate fibroblasts, could play a role in modulating non-HF SAN fibrotic content relative to RA. *Neat1*[38] may be more specific to TGFβ1 activation in RA fibroblasts but not to SAN cells (Figure 6B). Future studies should systematically investigate whether any uncharacterized lncRNAs in our data set contribute to SAN fibrotic content and serve as novel therapeutic targets to treat cardiac remodeling in HF.

Among miRNAs, miRNA-615-3p, miRNA-10b-3p, miRNA-10b-5p, and miRNA-1292-5p, previously associated with cancer and tumor progression,[39–41] were higher in the non-HF SAN compared with RA fibroblasts (Figure 6C). miRNA-1306-5p is known to be released by the myocardium, and its circulating levels are considered a biomarker of HF.[43] We found that miRNA-1306-5p is expressed in human SAN fibroblasts as well, with higher levels in untreated non-HF SAN fibroblasts. Network analyses also showed that many of the significantly different SAN miRNAs paired inversely with selected ECM and profibrotic genes, which predicted potential miRNA-mediated regulation of these genes and SAN fibrosis (Figure 7). Overall, these putative interactions could be used to identify candidate miRNAs to determine regulation of predicted fibrosis-associated mRNA targets in the SAN.

Although few studies have sequenced global proteomic profiles in the human heart,[43,44] proteomic profiling of human SAN fibroblasts has never been performed. We identified an average of ≈15 000 peptide spectral matches across all SAN and RA samples, demonstrating both similar and distinct profiles (Figure 8A). Expression patterns of many profibrotic and ECM proteins,

including LTBP2 and POSTN, indicate that common ECM and myofibroblast-associated signaling pathways are similarly regulated in both untreated and TGFβ1-treated non-HF and HF SAN and RA (Figure 8B). However, untreated non-HF SAN fibroblasts demonstrated proteomic signatures distinct from that of the non-HF RA, with increased expression in annexinA6, COL3A1, filamin B, STAT2, TLN1, and vinculin. In contrast, COL3A1 was lower in untreated HF SAN cells compared with RA. Higher COL3A1 could suggest a more flexible SAN ECM composition in non-HF versus HF. Overall, these results, along with those in Figure 2B and 2C, indicate that non-HF SAN fibroblasts may secrete proteins that promote flexibility in the ECM, which may decrease in HF, leading to a stiffer, less flexible composition in the HF SAN. Substrate stiffness is known to modulate TGFβ1 signaling by promoting myofibroblast transition,[45] thereby creating a positive feedback loop in fibrosis progression. Hence a shift toward stiffness in HF SAN ECM could promote myofibroblast differentiation and fibrosis within the SAN, similar to what we found in situ (Figure 4A). Moreover, findings from a porcine SAN ECM study identified both stiffer and elastic components, which could withstand higher tensile forces while reducing mechanical strain on pacemaker myocytes.[23] These findings suggest that a balance of both stiff and elastic ECM components may be necessary for optimal SAN function, which could be altered in the HF SAN. Whereas increases in mechanical stretch or intra-atrial pressure can increase SAN rhythm, compression or increased arterial blood pressure in SAN artery can slow rhythm.[46–48] A stiffer composition of the ECM in the HF SAN can impede this physiologic response to changes in atrial or arterial pressures. Studies to dissect the ECM protein composition in detail in non-HF and HF human SAN should allow us to confirm these fibroblast-specific findings in determining the role of in situ ECM composition in SAN automaticity and conduction abnormalities.

TGFβ1 induced a remarkably similar pattern of protein expression among most of the selected profibrotic/ECM genes in untreated non-HF SAN and RA fibroblasts, with the specific exception of COL3A1, which was upregulated in the non-HF SAN but not RA TGFβ1 cells (Figure 8B and 8C). These data suggest that activated non-HF SAN myofibroblasts may be different from their RA counterparts in secretion of COL3A1 associated with less rigid ECM properties. Upregulation of POSTN and LTBP2 in non-HF SAN fibroblasts and CADH2 and ITA4 in HF SAN fibroblasts after TGFβ1 may imply inherently different gene programs in untreated non-HF and HF cells that could in turn promote differentiation into distinct myofibroblasts. These protein signatures are also supported by gene ontology and KEGG analyses of SAN untreated versus TGFβ1 data sets (Figure 8D and 8E). Overall, our data suggest that relative to untreated fibroblasts, activated non-HF SAN myofibroblasts are prone to increased secretion of profibrotic proteins related to ECM and fibrosis, whereas HF SAN myofibroblasts suggest pathologic phenotypes consistent with cardiomyopathy.

Limitations

Our study was performed on a relatively small sample of intact adult, primarily male human SANs and HF hearts, which may not be representative of all human hearts. Noncardiac comorbidities and lifestyle modifications, including alcohol consumption and drug abuse, as well as presence of implanted cardiac devices and SAN dysfunction in the HF group may affect the results. Based on the availability of ex vivo hearts for SAN tissue and cell collection[49] at The Ohio State University, we used donor hearts with complete SAN pacemaker complex without cardiac dysfunction for the nonfailing group and failing hearts from transplant surgeries for the HF group. Only those samples that met quality control and all inclusion criteria were retained for analyses (Figure IV in the Data Supplement).

Conclusions

In human HF SAN, proliferating fibroblasts, myofibroblasts, ECM with stiffer properties, and POSTN-positive fibrotic islands increase, which creates intranodal structural barriers that could interrupt normal automaticity and conduction. In non-HF SAN fibroblasts, molecular and protein markers are different from RA fibroblasts, which predispose to SAN-specific impairments in ECM flexibility and myofibroblast differentiation. This comprehensive atlas of molecular and protein targets establishes a valuable human SAN fibroblast-specific proteo–whole transcriptome database that can be used to identify molecular and protein signatures, signaling pathways, and potential therapeutic targets of SAN fibrosis and cardiac arrhythmias in patients with HF.

ARTICLE INFORMATION

Received September 28, 2020; accepted March 26, 2021.

Affiliations

Department of Physiology & Cell Biology (A.K., N.L., E.J.A., B.J.H., P.M.L.J., P.J.M., V.V.F.), Bob and Corrine Frick Center for Heart Failure and Arrhythmia, Dorothy M. Davis Heart & Lung Research Institute (A.K., N.L., E.J.A., B.J.H., P.J.M., V.V.F.), Cancer Biology and Genetics (M.L.G., M.A.F.), Biomedical Informatics Shared Resources (A.W., M.P.), and Department of Surgery (B.A.W., N.A.M.), The Ohio State University Wexner Medical Center, Columbus.

Acknowledgments

The authors thank the Lifeline of Ohio Organ Procurement Organization and the Division of Cardiac Surgery, Ohio State University Wexner Medical Center, for providing explanted hearts; the Campus Microscopy and Imaging Facility, The Ohio State University (National Cancer Institute grant P30 CA016058); Campus Chemical Instrument Center Mass Spectrometry and Proteomics shared resource, The Ohio State University (National Institutes of Health grants P30 CA016058 and S10 OD018056); Dr Patrick Stevens, Biomedical Informatics

Shared Resource, The Ohio State University; Dr Lisa Dorn (Accornero Laboratory); Dr Nehal Patel (Hund Laboratory); and members of Janssen and Fedorov Labs for providing assistance during the project.

Sources of Funding

This work was supported by grants from the National Institutes of Health (HL115580, HL135109, HL142179, HL134824, and HL135754), Leducq Foundation (TNE FANTASY 19CVD03), and the Bob and Corrine Frick Center for Heart Failure and Arrhythmia, The Ohio State University.

Disclosures

None.

Supplemental Materials

Expanded Methods
Data Supplement Figures I–XVI
Data Supplement Tables I–VIII
Data Supplement Excel Files I–IX

REFERENCES

1. Csepe TA, Zhao J, Hansen BJ, Li N, Sul LV, Lim P, Wang Y, Simonetti OP, Kilic A, Mohler PJ, et al. Human sinoatrial node structure: 3D microanatomy of sinoatrial conduction pathways. *Prog Biophys Mol Biol.* 2016;120:164–178. doi: 10.1016/j.pbiomolbio.2015.12.011
2. Opthof T, de Jonge B, Jongsma HJ, Bouman LN. Functional morphology of the mammalian sinuatrial node. *Eur Heart J.* 1987;8:1249–1259. doi: 10.1093/oxfordjournals.eurheartj.a062200
3. Keith A, Flack M. The form and nature of the muscular connections between the primary divisions of the vertebrate heart. *J Anat Physiol.* 1907;41:172–189.
4. Csepe TA, Kalyanasundaram A, Hansen BJ, Zhao J, Fedorov VV. Fibrosis: a structural modulator of sinoatrial node physiology and dysfunction. *Front Physiol.* 2015;6:37. doi: 10.3389/fphys.2015.00037
5. Csepe TA, Zhao J, Sul LV, Wang Y, Hansen BJ, Li N, Ignozzi AJ, Bratasz A, Powell KA, Kilic A, et al. Novel application of 3D contrast-enhanced CMR to define fibrotic structure of the human sinoatrial node in vivo. *Eur Heart J Cardiovasc Imaging.* 2017;18:862–869. doi: 10.1093/ehjci/jew304
6. Shiraishi I, Takamatsu T, Minamikawa T, Onouchi Z, Fujita S. Quantitative histological analysis of the human sinoatrial node during growth and aging. *Circulation.* 1992;85:2176–2184. doi: 10.1161/01.cir.85.6.2176
7. Kalyanasundaram A, Li N, Hansen BJ, Zhao J, Fedorov VV. Canine and human sinoatrial node: differences and similarities in the structure, function, molecular profiles, and arrhythmia. *J Vet Cardiol.* 2019;22:2–19. doi: 10.1016/j.jvc.2018.10.004
8. Lou Q, Hansen BJ, Fedorenko O, Csepe TA, Kalyanasundaram A, Li N, Hage LT, Glukhov AV, Billman GE, Weiss R, et al. Upregulation of adenosine A1 receptors facilitates sinoatrial node dysfunction in chronic canine heart failure by exacerbating nodal conduction abnormalities revealed by novel dual-sided intramural optical mapping. *Circulation.* 2014;130:315–324. doi: 10.1161/CIRCULATIONAHA.113.007086
9. Sanders P, Kistler PM, Morton JB, Spence SJ, Kalman JM. Remodeling of sinus node function in patients with congestive heart failure: reduction in sinus node reserve. *Circulation.* 2004;110:897–903. doi: 10.1161/01.CIR.0000139336.69955.AB
10. Li N, Hansen BJ, Csepe TA, Zhao J, Ignozzi AJ, Sul LV, Zakharkin SO, Kalyanasundaram A, Davis JP, Biesiadecki BJ, et al. Redundant and diverse intranodal pacemakers and conduction pathways protect the human sinoatrial node from failure. *Sci Transl Med.* 2017;9:eaam5607. doi: 10.1126/scitranslmed.aam5607
11. Li N, Kalyanasundaram A, Hansen BJ, Artiga EJ, Sharma R, Abudulwahed SH, Helfrich KM, Rozenberg G, Wu PJ, Zakharkin S, et al. Impaired neuronal sodium channels cause intranodal conduction failure and reentrant arrhythmias in human sinoatrial node. *Nat Commun.* 2020;11:512. doi: 10.1038/s41467-019-14039-8
12. Humeres C, Frangogiannis NG. Fibroblasts in the infarcted, remodeling, and failing heart. *JACC Basic Transl Sci.* 2019;4:449–467. doi: 10.1016/j.jacbts.2019.02.006
13. Frangogiannis NG. Cardiac fibrosis: cell biological mechanisms, molecular pathways and therapeutic opportunities. *Mol Aspects Med.* 2019;65:70–99. doi: 10.1016/j.mam.2018.07.001
14. Edgar R, Domrachev M, Lash AE. Gene Expression Omnibus: NCBI gene expression and hybridization array data repository. *Nucleic Acids Res.* 2002;30:207–210. doi: 10.1093/nar/30.1.207
15. Hobuß L, Bär C, Thum T. Long non-coding RNAs: at the heart of cardiac dysfunction? *Front Physiol.* 2019;10:30. doi: 10.3389/fphys.2019.00030
16. Micheletti R, Plaisance I, Abraham BJ, Sarre A, Ting CC, Alexanian M, Maric D, Maison D, Nemir M, Young RA, et al. The long noncoding RNA Wisper controls cardiac fibrosis and remodeling. *Sci Transl Med.* 2017;9:eaai9118. doi: 10.1126/scitranslmed.aai9118
17. Peters T, Hermans-Beijnsberger S, Beqqali A, Bitsch N, Nakagawa S, Prasanth KV, de Windt LJ, van Oort RJ, Heymans S, Schroen B. Long noncoding RNA malat-1 is dispensable during pressure overload-induced cardiac remodeling and failure in mice. *PLoS One.* 2016;11:e0150236. doi: 10.1371/journal.pone.0150236
18. Tallquist MD, Molkentin JD. Redefining the identity of cardiac fibroblasts. *Nat Rev Cardiol.* 2017;14:484–491. doi: 10.1038/nrcardio.2017.57
19. Travers JG, Kamal FA, Robbins J, Yutzey KE, Blaxall BC. Cardiac fibrosis: the fibroblast awakens. *Circ Res.* 2016;118:1021–1040. doi: 10.1161/CIRCRESAHA.115.306565
20. van Nieuwenhoven FA, Munts C, Op't Veld RC, González A, Díez J, Heymans S, Schroen B, van Bilsen M. Cartilage intermediate layer protein 1 (CILP1): A novel mediator of cardiac extracellular matrix remodelling. *Sci Rep.* 2017;7:16042. doi: 10.1038/s41598-017-16201-y
21. Zhao S, Wu H, Xia W, Chen X, Zhu S, Zhang S, Shao Y, Ma W, Yang D, Zhang J. Periostin expression is upregulated and associated with myocardial fibrosis in human failing hearts. *J Cardiol.* 2014;63:373–378. doi: 10.1016/j.jjcc.2013.09.013
22. Oka T, Xu J, Kaiser RA, Melendez J, Hambleton M, Sargent MA, Lorts A, Brunskill EW, Dorn GW II, Conway SJ, et al. Genetic manipulation of periostin expression reveals a role in cardiac hypertrophy and ventricular remodeling. *Circ Res.* 2007;101:313–321. doi: 10.1161/CIRCRESAHA.107.149047
23. Gluck JM, Herren AW, Yechikov S, Kao HKJ, Khan A, Phinney BS, Chiamvimonvat N, Chan JW, Lieu DK. Biochemical and biomechanical properties of the pacemaking sinoatrial node extracellular matrix are distinct from contractile left ventricular matrix. *PLoS One.* 2017;12:e0185125. doi: 10.1371/journal.pone.0185125
24. Camelliti P, Green CR, LeGrice I, Kohl P. Fibroblast network in rabbit sinoatrial node: structural and functional identification of homogeneous and heterogeneous cell coupling. *Circ Res.* 2004;94:828–835. doi: 10.1161/01.RES.0000122382.19400.14
25. Nagaraju CK, Robinson EL, Abdesselem M, Trenson S, Dries E, Gilbert G, Janssens S, Van Cleemput J, Rega F, Meyns B, et al. Myofibroblast phenotype and reversibility of fibrosis in patients with end-stage heart failure. *J Am Coll Cardiol.* 2019;73:2267–2282. doi: 10.1016/j.jacc.2019.02.049
26. Fu X, Khalil H, Kanisicak O, Boyer JG, Vagnozzi RJ, Maliken BD, Sargent MA, Prasad V, Valiente-Alandi I, Blaxall BC, et al. Specialized fibroblast differentiated states underlie scar formation in the infarcted mouse heart. *J Clin Invest.* 2018;128:2127–2143. doi: 10.1172/JCI98215
27. Schafer S, Viswanathan S, Widjaja AA, Lim WW, Moreno-Moral A, DeLaughter DM, Ng B, Patone G, Chow K, Khin E, et al. IL-11 is a crucial determinant of cardiovascular fibrosis. *Nature.* 2017;552:110–115. doi: 10.1038/nature24676
28. Frey N, Richardson JA, Olson EN. Calsarcins, a novel family of sarcomeric calcineurin-binding proteins. *Proc Natl Acad Sci U S A.* 2000;97:14632–14637. doi: 10.1073/pnas.260501097
29. Gladka MM, Molenaar B, de Ruiter H, van der Elst S, Tsui H, Versteeg D, Lacraz GPA, Huibers MMH, van Oudenaarden A, van Rooij E. Single-cell sequencing of the healthy and diseased heart reveals cytoskeleton-associated protein 4 as a new modulator of fibroblasts activation. *Circulation.* 2018;138:166–180. doi: 10.1161/CIRCULATIONAHA.117.030742
30. Osio A, Tan L, Chen SN, Lombardi R, Nagueh SF, Shete S, Roberts R, Willerson JT, Marian AJ. Myozenin 2 is a novel gene for human hypertrophic cardiomyopathy. *Circ Res.* 2007;100:766–768. doi: 10.1161/01.RES.0000263008.66799.aa
31. Alexanian M, Przytycki PF, Micheletti R, Padmanabhan A, Ye L, Travers JG, Teran BG, Duan Q, Ranade SS, Felix F, et al. A transcriptional switch governing fibroblast plasticity underlies reversibility of chronic heart disease. *bioRxiv.* Preprint posted online July 22, 2020. doi: 10.1101/2020.07.21.214874
32. Leight JL, Wozniak MA, Chen S, Lynch ML, Chen CS. Matrix rigidity regulates a switch between TGF-β1-induced apoptosis and epithelial-mesenchymal transition. *Mol Biol Cell.* 2012;23:781–791. doi: 10.1091/mbc.E11-06-0537
33. Zhu Y, Feng Z, Jian Z, Xiao Y. Long noncoding RNA TUG1 promotes cardiac fibroblast transformation to myofibroblasts via miR-29c in chronic hypoxia. *Mol Med Rep.* 2018;18:3451–3460. doi: 10.3892/mmr.2018.9327

34. Piccoli MT, Bär C, Thum T. Non-coding RNAs as modulators of the cardiac fibroblast phenotype. *J Mol Cell Cardiol.* 2016;92:75–81. doi: 10.1016/j.yjmcc.2015.12.023
35. Thum T. Noncoding RNAs and myocardial fibrosis. *Nat Rev Cardiol.* 2014;11:655–663. doi: 10.1038/nrcardio.2014.125
36. McKinsey TA, Vondriska TM, Wang Y. Epigenomic regulation of heart failure: integrating histone marks, long noncoding RNAs, and chromatin architecture. *F1000Res.* 2018;7:1713. doi: 10.12688/f1000research.15797.1
37. Tao H, Zhang JG, Qin RH, Dai C, Shi P, Yang JJ, Deng ZY, Shi KH. LncRNA GAS5 controls cardiac fibroblast activation and fibrosis by targeting miR-21 via PTEN/MMP-2 signaling pathway. *Toxicology.* 2017;386:11–18. doi: 10.1016/j.tox.2017.05.007
38. Kenneweg F, Bang C, Xiao K, Boulanger CM, Loyer X, Mazlan S, Schroen B, Hermans-Beijnsberger S, Foinquinos A, Hirt MN, et al. Long noncoding RNA-enriched vesicles secreted by hypoxic cardiomyocytes drive cardiac fibrosis. *Mol Ther Nucleic Acids.* 2019;18:363–374. doi: 10.1016/j.omtn.2019.09.003
39. Yan T, Ooi WF, Qamra A, Cheung A, Ma D, Sundaram GM, Xu C, Xing M, Poon L, Wang J, et al. HoxC5 and miR-615-3p target newly evolved genomic regions to repress hTERT and inhibit tumorigenesis. *Nat Commun.* 2018;9:100. doi: 10.1038/s41467-017-02601-1
40. Han X, Yan S, Weijie Z, Feng W, Liuxing W, Mengquan L, Qingxia F. Critical role of miR-10b in transforming growth factor-β1-induced epithelial-mesenchymal transition in breast cancer. *Cancer Gene Ther.* 2014;21:60–67. doi: 10.1038/cgt.2013.82
41. Hui W, Ma X, Zan Y, Song L, Zhang S, Dong L. MicroRNA-1292-5p inhibits cell growth, migration and invasion of gastric carcinoma by targeting DEK. *Am J Cancer Res.* 2018;8:1228–1238.
42. van Boven N, Kardys I, van Vark LC, Akkerhuis KM, de Ronde MWJ, Khan MAF, Merkus D, Liu Z, Voors AA, Asselbergs FW, et al. Serially measured circulating microRNAs and adverse clinical outcomes in patients with acute heart failure. *Eur J Heart Fail.* 2018;20:89–96. doi: 10.1002/ejhf.950
43. Sebastião MJ, Pereira R, Serra M, Gomes-Alves P, Alves PM. Unveiling human cardiac fibroblast membrane proteome. *Proteomics.* 2018;18:e1700446. doi: 10.1002/pmic.201700446
44. Doll S, Dreßen M, Geyer PE, Itzhak DN, Braun C, Doppler SA, Meier F, Deutsch MA, Lahm H, Lange R, et al. Region and cell-type resolved quantitative proteomic map of the human heart. *Nat Commun.* 2017;8:1469. doi: 10.1038/s41467-017-01747-2
45. Herum KM, Lunde IG, McCulloch AD, Christensen G. The soft- and hard-heartedness of cardiac fibroblasts: mechanotransduction signaling pathways in fibrosis of the heart. *J Clin Med.* 2017;6:E53. doi: 10.3390/jcm6050053
46. Hashimoto K, Tanaka S, Hirata M, Chiba S. Responses of the sino-atrial node to change in pressure in the sinus node artery. *Circ Res.* 1967;21:297–304. doi: 10.1161/01.res.21.3.297
47. James TN, Nadeau RA. Direct perfusion of the sinus node: an experimental model for pharmacologic and electrophysiologic studies of the heart. *Henry Ford Hosp Med Bull.* 1962;10:21–25.
48. Lange G, Lu HH, Chang A, Brooks CM. Effect of stretch on the isolated cat sinoatrial node. *Am J Physiol.* 1966;211:1192–1196. doi: 10.1152/ajplegacy.1966.211.5.1192
49. Mikhailov AV, Kalyanasundaram A, Li N, Scott SS, Artiga EJ, Subr MM, Zhao J, Hansen BJ, Hummel JD, Fedorov VV. Comprehensive evaluation of electrophysiological and 3D structural features of human atrial myocardium with insights on atrial fibrillation maintenance mechanisms. *J Mol Cell Cardiol.* 2021;151:56–71. doi: 10.1016/j.yjmcc.2020.10.012